applied sciences

MDPI

Article

Research on Tree Flash Fault Localization of Hybrid Overhead–Underground Lines Based on Improved Double-Ended Traveling Wave Method

Zukang Huang, Chunhua Fang *, Quancai Jiang, Tao Hu and Junjie Lv

College of Electricity and New Energy, Three Gorges University, Yichang 443002, China; fang107531@163.com (Z.H.); qcjiang@ctgu.edu.cn (Q.J.); 202108580021094@ctgu.edu.cn (T.H.); 202108580021180@ctgu.edu.cn (J.L.)
* Correspondence: ctgu0402@126.com

Abstract: The occurrence of tree flash faults in hybrid overhead–underground lines presents a significant challenge to the smooth operation of power systems. However, research on localizing such faults is relatively scarce. This study conducts theoretical analyses on the formation of tree flash faults, constructs a tree flash fault discharge test platform, and simulates the discharge process. The tree flash fault discharge traveling wave signals were obtained through a high-frequency current acquisition system. Additionally, this paper establishes a model for the current traveling wave of tree flash faults and analyzes transmission attenuation. To enhance the bi-terminal traveling wave localization method, we introduce modal decomposition and the Hilbert–Huang transform. Modal decomposition is used to disentangle signals and derive the instantaneous frequencies of modal signal components through the Hilbert–Huang transform. This process helps determine the time at which the initial wavefront reaches the terminals of the mixed-line transmission. The simulation analysis carried out using PSCAD/EMTDC v4.6.3 demonstrates that this method effectively calibrates the wavefront timing of tree flash fault signals without requiring knowledge of their wave velocity along the mixed-line transmission. Therefore, this approach achieves precise localization of tree flash faults efficiently.

Keywords: double-end traveling wave method; fault localization; Hilbert–Huang transform (HHT); hybrid line; tree flash fault; variational mode decomposition (VMD)

Citation: Huang, Z.; Fang, C.; Jiang, Q.; Hu, T.; Lv, J. Research on Tree Flash Fault Localization of Hybrid Overhead–Underground Lines Based on Improved Double-Ended Traveling Wave Method. *Appl. Sci.* **2024**, *14*, 4739. https://doi.org/10.3390/app14114739

Academic Editors: Akhtar Kalam, Filipe Soares and Seyed Morteza Alizadeh

Received: 24 March 2024
Revised: 22 May 2024
Accepted: 27 May 2024
Published: 30 May 2024

1. Introduction

As the scale of power transmission and distribution systems, as well as power facilities, continues to expand, the number of hybrid overhead–underground lines in the power supply network is also increasing. High-voltage transmission lines are susceptible to external factors such as wind, rain, lightning, and internal faults, leading to power system failures. The occurrence of grounding faults in power systems due to direct or indirect contact between trees and transmission lines is referred to as "tree-flash faults" [1–3]. For instance, in 2016, a major power outage occurred in South Australia, Australia, affecting approximately 750,000 users. One of the causes of the outage was intense tornadoes and lightning strikes, which led to trees collapsing and ultimately resulted in short circuits in the transmission lines, causing the power outage [4]. When a tree flash fault occurs in hybrid overhead–underground lines, it is crucial to promptly determine the precise location of the fault. This is of significant importance for swiftly rectifying the fault, ensuring the smooth operation of the power system, and enhancing the reliability of the supply system.

Research on tree flash faults requires the full utilization of sensing technology, data collection, and analytical methods. By integrating advanced sensors and intelligent algorithms, real-time monitoring and analysis of tree flash faults can be achieved, driving the

development of the power system toward intelligence. With the rapid development of new energy sources and the continuous evolution of electricity demand, power systems require more flexible and reliable solutions [5]. Researchers have conducted relevant studies on tree flash faults and have obtained corresponding results. John Goodfellow [6] not only delves into the in-depth exploration of tree structure and growth characteristics but also includes a comprehensive assessment of potential risk factors. Chau Wai Yi et al. [7] proposed a tree tilt monitoring solution based on an AI-IoT integrated framework, aiming to prevent tree collapse accidents in advance and enhance urban forestry safety. Long Yue Zhang et al. [8] proposed a method to identify vegetation-related failure collapse sequences and their timescales by simulating the dynamic behavior of line sag and vegetation growth. This provides important insights for predicting and preventing tree-related failures. Ali Jahani et al. [9] compared the effectiveness of different models in predicting the collapse of Platanus orientalis trees in urban forests and proposed a prediction model based on a Support Vector Machine (SVM), providing urban forest managers with an effective tool for ecological failure risk assessment. Zhenyao Liu et al. [10] analyzed the mechanism of tree fault occurrence and simulated the discharge process between trees and transmission lines in a laboratory environment, revealing the changing characteristics of discharges when trees approach transmission lines. Mohammad Sadegh Bashkari et al. [11] analyzed distribution network outage data to identify the primary factors leading to vegetation-related outages and extracted relevant features. A. U. Melagoda et al. [12] proposed a data-driven approach to predict vegetation-related outages in power distribution systems, utilizing machine learning methods for prediction, and developed a real-time outage prediction platform. Nooshin Bahador et al. [13] conducted a study based on experimental data to investigate high-impedance faults (HIFs) caused by trees and proposed a new mathematical model to illustrate the influence of environmental conditions and biological classification. Nooshin Bahador et al. [14] proposed a new single-ended localization method based on non-contact magnetic field strength measurement for tree-related high-impedance faults. V. Ashok et al. [15] proposed a fault diagnosis scheme for tree flash fault syndrome associated with cross-country faults (CCFs).

Common methods for hybrid line fault localization include fault parameter analysis, intelligent algorithms, and traveling wave methods. The fault parameter analysis method typically provides high localization accuracy. When considering multiple parameters comprehensively, it can more accurately determine the fault location. However, it relies on data quality and is greatly affected by system complexity [16,17]. For instance, Bikash Patel [18] proposed a novel digital relay protection system for fault localization on hybrid transmission lines, featuring rapid and accurate fault location without the need for prior identification of the faulty section. Intelligent algorithms possess efficient capabilities in data processing, pattern recognition, and solving optimization problems. They are not only capable of handling vast amounts of power system data but also of uncovering potential correlations and patterns within it [19,20]. For instance, Zakaria El Mrabet et al. [21] proposed a data-driven method that utilizes fault trajectory samples to determine the fault location and employs a Random Forest Regressor (RFR) model for real-time detection of fault location and duration. The traveling wave method processes data relatively quickly and can complete fault location tasks in a short time. However, the accuracy of fault location is affected by the arrival time and velocity of transient wavefronts, thus influencing the precision of localization [22,23]. For instance, Jian Wang et al. [24] analyzed fault traveling waves on LCC-MMC HVDC transmission lines and proposed a fault localization principle based on the modal traveling wave arrival time difference and the ratio of fault traveling wave propagation paths. Jiali Ding et al. [25] introduced a novel traveling-wave-based fault-location algorithm for multiterminal transmission lines. Overall, the integration of algorithms with traveling wave methods improves the accuracy and real-time performance of fault localization, making fault localization in hybrid systems more efficient and reliable.

Determining the arrival time and velocity of fault traveling wave heads in fault location can be achieved using the traveling wave method. Lei Wang et al. [26] use variational mode

decomposition (VMD) and the Teager energy operator (TEO) to detect traveling wave faults through fault signals. Naidu et al. [27] proposed a traveling-wave-based fault localization method for two-terminal transmission lines, utilizing asynchronous current measurement data recorded by Intelligent Electronic Devices (IEDs) at both ends. Felipe V. Lopes et al. [28] proposed a traveling-wave-based solution for time synchronization of two-terminal data on transmission lines, estimating the arrival times of modal traveling waves at both ends through analysis of line energization or fault records with high sampling rates. Kun Yu et al. [29] proposed a novel traveling wave fault location method based on time linear dependence, utilizing the proximal point optimization algorithm (PPOA) to identify the shortest transmission path of the fault traveling wave. However, this method is still susceptible to various abnormal conditions, such as faults in the traveling wave location device, startup failures, and time recording errors, which may lead to inaccurate fault localization. Chenhao Zhang et al. [30] employed a single-ended traveling wave fault location technique based on waveform fitting, which effectively eliminates errors and provides accurate fault locations and impedance information. However, it may be sensitive to changes in fault types and modes, necessitating further testing and validation.

Currently, research on tree flash faults primarily focuses on prevention, handling, and diagnosis, with limited studies specifically addressing tree flash fault localization. Understanding the formation process of tree flash faults is crucial for researching their localization. After analyzing the formation process of tree flash faults, this paper established a tree flash fault discharge test platform to capture tree flash fault discharge current waveforms through experiments, constructed a tree flash fault traveling wave model, and facilitated subsequent simulation studies. The Variational Mode Decomposition (VMD) algorithm, known for its superior ability to extract local frequency characteristics compared to other decomposition methods like wavelet transform, was utilized alongside the Hilbert transform and a bi-terminal localization algorithm independent of wave velocity to achieve tree flash fault localization. Through PSCAD/EMTDC simulations, the effectiveness of this localization method was validated.

2. Theoretical Analysis of Tree Flash Fault Formation in Hybrid Transmission Lines

Schematic of Tree Flash Fault Occurrence Process (see Figure 1). L represents the height of the tree; h represents the height of the transmission line tower; f_0, f_1, and f_2 represent the sag distance of the conductor; and d represents the safety distance.

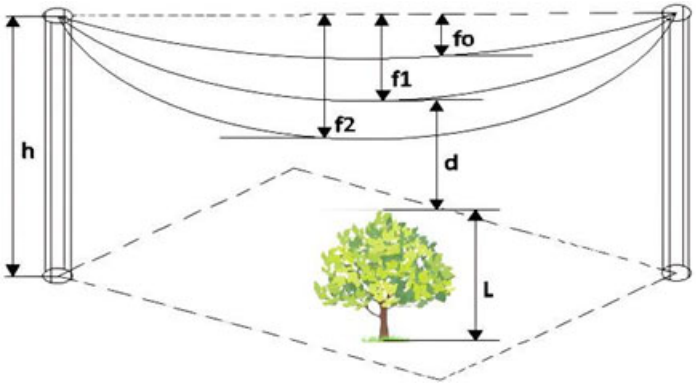

Figure 1. Illustration of tree flash fault occurrence.

Specifically, f_0 refers to the initial sag distance of the conductors in normal operating conditions. When the conductors are affected by external environmental factors and self-heating, leading to an increase in conductor temperature and length, the sag distance also increases accordingly. At this point, the sag distance may increase to f_1 and eventually reach f_2 as the severity of the conditions intensifies. At the same time, when the height of the trees directly below or on both sides of the overhead transmission lines reaches due to

rapid growth and lack of timely trimming, and the clearance distance between the trees and the conductors is less than the safety distance L, the transmission conductors will discharge electricity to the trees, leading to the occurrence of tree flash faults. The critical condition for the occurrence of tree flash faults is denoted as $L \geq h - f - d$.

The critical condition $L \geq h - f - d$ ensures a safe distance between trees and power lines. When the critical condition is not met, i.e., when $L < h - f - d$, the distance between trees and power lines is too close, posing the risk of discharge from the power lines to the trees, which may lead to tree flash faults. Adhering to the critical condition helps prevent tree flash faults and ensures the safe operation of overhead transmission lines. The meaning of key conditions: L: The net clearance distance between trees and power lines, representing the shortest distance between trees and power lines under conditions of tree growth and changes in wire sag. h: The height of trees, serving as a crucial parameter for measuring the vertical distance between trees and power lines. f: The sag of power lines, indicating the vertical downward distance of power lines, influenced by external environmental factors and the weight of the power lines themselves. d: The safety distance, referring to the minimum net clearance distance between power lines and trees, ensuring the prevention of tree flash faults under various conditions. The establishment of safety distance d is crucial to ensure a safe distance between power lines and the surrounding environment, especially trees, thereby preventing potential electrical discharge and tree flash faults.

3. Research on Tree Flash Fault Discharge Experiments

3.1. Establishment of an Experimental Platform

To obtain the waveform of the tree flash fault discharge current, we first established a tree flash fault discharge test platform (see Figure 2). The numbered items in the diagram are as follows: 1. Protective resistor. 2. Insulating rope. 3. Insulator. 4. Simulated conductor. 5. High-frequency current sensor. 6. Tree. 7. Camera. 8. HS5 high-speed data acquisition card. 9. Computer. *T*1 is the voltage regulator, and *T*2 is the test transformer; *C*1 and *C*2 are voltage divider capacitors with a ratio of 1:10,000. In the voltage boosting system, the voltage regulator is a column-type motorized voltage regulator with input/output frequencies of 50 Hz/60 Hz. The rated capacity of the test transformer for tree flash fault discharge experiments is 50 kVA, and the protective resistor is 10 kV. The simulated conductor chosen is a steel-cored aluminum-stranded wire with the model LGJ-630/45 (Jinlong Cable Technology Co., Ltd., Changsha, China). The high-speed HS5 extracts the current waveform and current amplitude characteristics of the experimentally simplified conductor in the circuit.

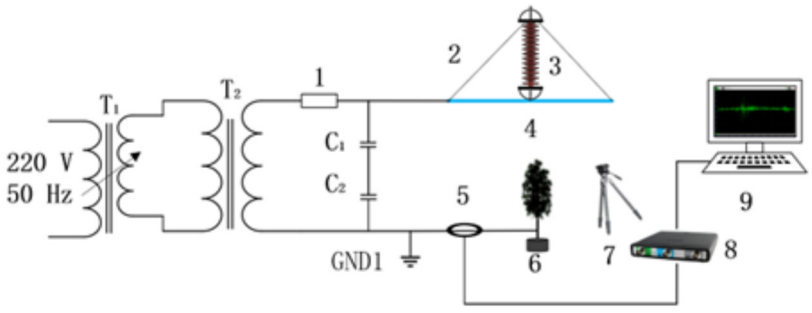

Figure 2. Schematic diagram of the tree flash fault discharge test platform.

3.2. Experimental Method

Firstly, arrange all equipment in the high-voltage test laboratory according to the schematic diagram of the test platform. Considering the extreme imbalance between the spacing of trees and conductors within specific spacing areas, their distances have a linear correlation with the breakdown current intensity. Taking 4 kV/cm as a reference for the breakdown current intensity and calculating it with a voltage of 100 kV, the maximum clearance distance between trees and conductors will reach 25 cm [31]. If this safety

distance is exceeded, it may lead to tree flash fault discharge problems. Place the required trees directly below the simulated conductors, maintaining a 25 cm gap. Then, gradually increase the voltage using a step-up method until a bright arc occurs at the top of the tree, with the entire process being recorded by a camera. Finally, trigger the protection action of the test transformer, and shut down the tree flash fault discharge test platform. The data acquisition card collects the discharge current waveform, which is stored on the computer, and multiple tests are conducted to record the optimal results.

To accurately capture the current waveform of tree flash faults, the HS5 parameters are first set appropriately using a computer. Without any external voltage, we detect noise generated by the device itself or present in the environment, which may introduce interference in the waveform. Through statistical feature analysis of these interference waveforms, we adjust the corresponding parameters to ensure that the device collects data without false triggering. It should be noted that the occurrence of tree flash faults ultimately involves corona discharge. Since the current amplitude of corona discharge is much smaller than that of tree flash discharge, we only need to extract the waveform with the maximum discharge current amplitude from the collected data, which can be identified as the waveform of tree flash fault discharge. This method helps ensure that the collected data is relevant to tree flash faults, thus accurately recording the current waveform of tree flash faults.

3.3. Experimental Phenomena Analysis

According to the experimental method, gradually increasing the voltage revealed that when the voltage reached between 90 kV and 120 kV, a crisp buzzing sound emanated from the top of the tree. Simultaneously, a gradually brightening electric flame formed between the tree top and the simulated conductor (see Figure 3).

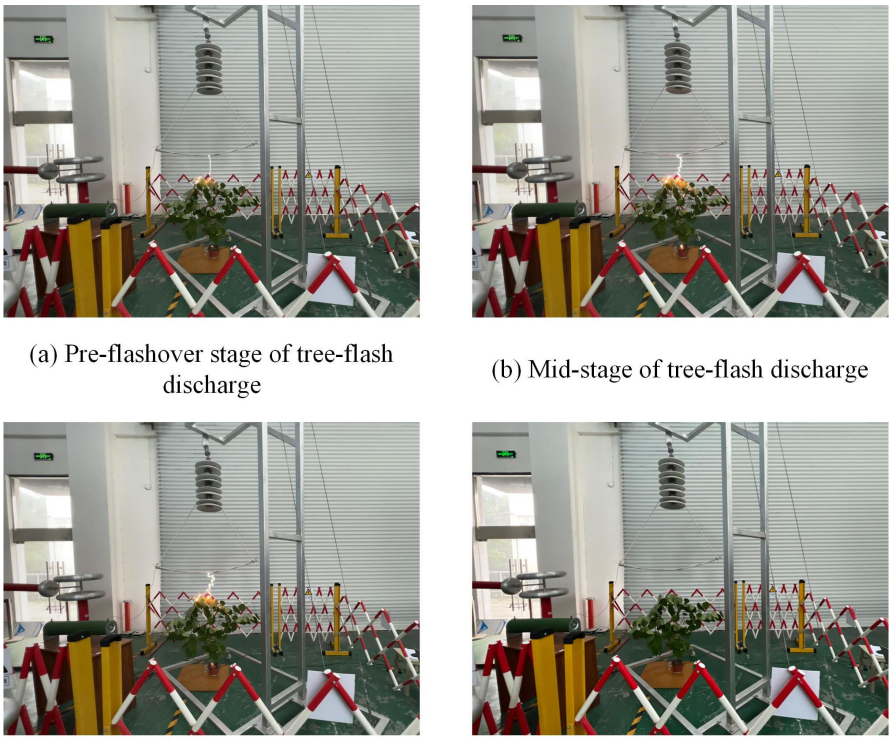

(a) Pre-flashover stage of tree-flash discharge

(b) Mid-stage of tree-flash discharge

(c) Late stage of tree-flash discharge

(c) End of tree-flash discharge

Figure 3. Tree flash fault discharge process.

The duration of the electric flame was very short, dissipating eventually. At this moment, the protection of the test transformer was activated, and the voltage was disconnected. During the occurrence of the tree flash fault, a bright electric flame formed,

accompanied by a pungent burning smell. Upon disconnecting the test device, an examination of the top of the tree revealed clear signs of scorching compared to its initial state.

3.4. Analysis of Tree Flash Fault Discharge Waveform

Multiple experiments collected a large number of waveforms of tree flash fault discharges. Typical discharge waveforms are shown in Figures 4–7, with voltage values applied by the boosting system at the time of protective action of the test transformer being 92 kV, 103 kV, 110 kV, and 118 kV, respectively. The peak-to-peak values and the main waveform widths of each waveform are shown in Table 1. The sampling frequency of data acquisition card HS5 was set to 20 MHz, with a sampling time of 400 μs, 8000 sampling points, and a sampling interval of 0.05 μs. During the tree flash fault discharge process, the current waveform contains high-frequency components. Setting a higher sampling frequency ensures capturing sufficient high-frequency information to accurately capture the details and rapid changes during the discharge process. To accurately reconstruct the signal, the sampling frequency should be at least twice the signal frequency. Since tree flash fault discharge involves high-frequency components, a sampling frequency of 20 MHz effectively avoids signal distortion and aliasing effects. A high sampling rate provides richer data, facilitating subsequent signal analysis and processing. In tree flashover fault studies, a high sampling rate can provide more accurate current waveform characteristics, aiding in a thorough analysis of the discharge process. In summary, setting the sampling frequency of the HS5 acquisition card to 20 MHz ensures the full capture of high-frequency signals during tree flash fault discharge experiments, thereby providing more accurate and comprehensive data for subsequent analysis and research.

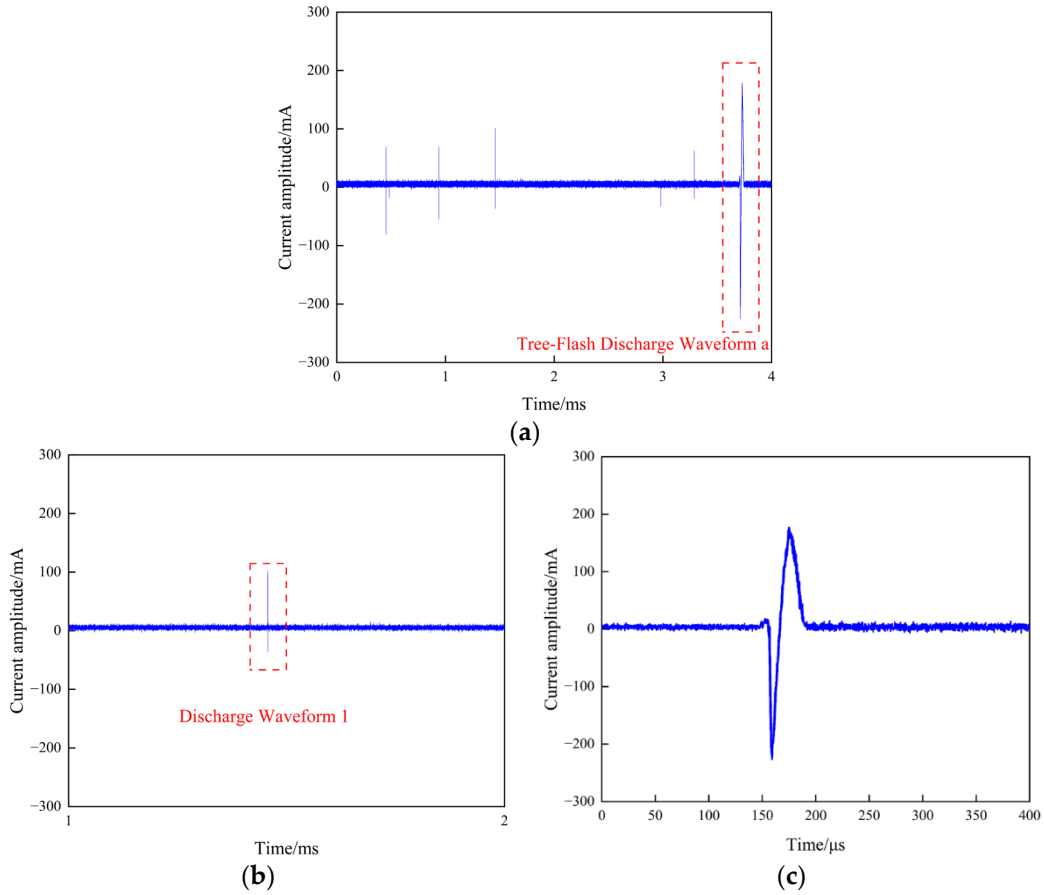

Figure 4. Tree flash fault test discharge current waveform (voltage value of booster system: 93 kV). (**a**) Raw current waveform plot; (**b**) magnified view of waveform; (**c**) tree flash discharge waveform a.

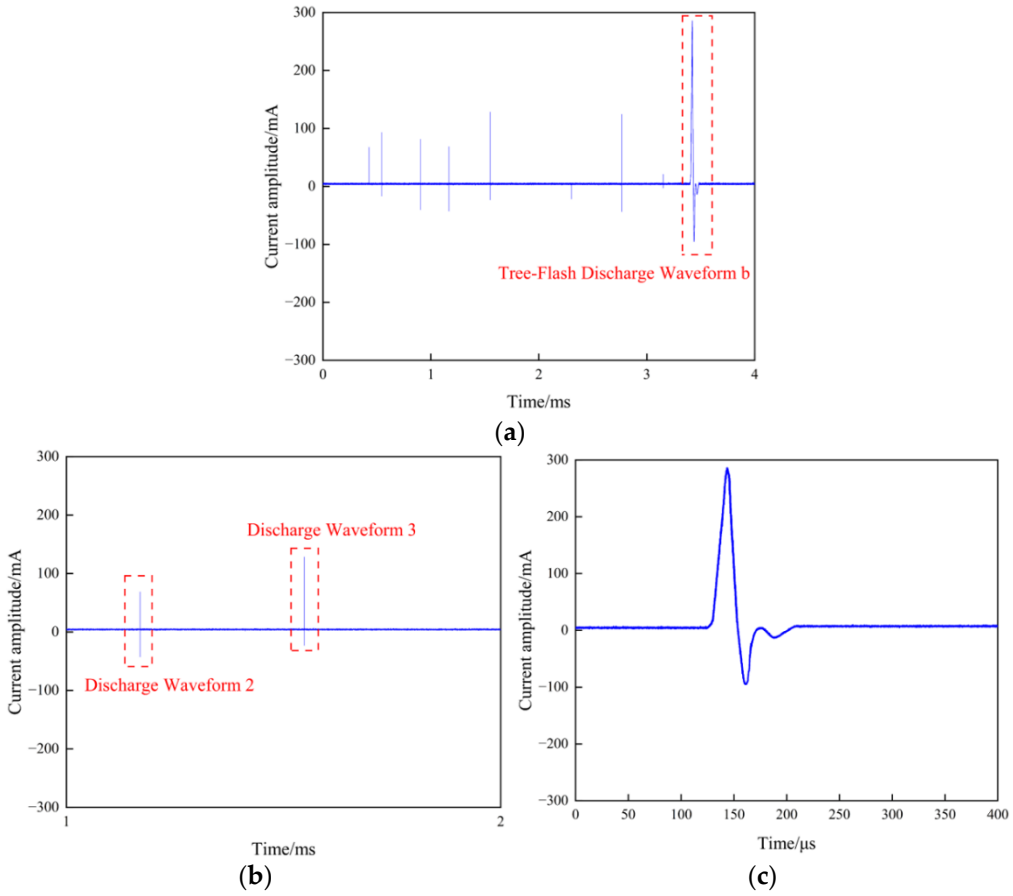

Figure 5. Tree flash fault test discharge current waveform (voltage value of booster system: 103 kV). (**a**) Raw current waveform plot; (**b**) magnified view of waveform; (**c**) tree flash discharge waveform b.

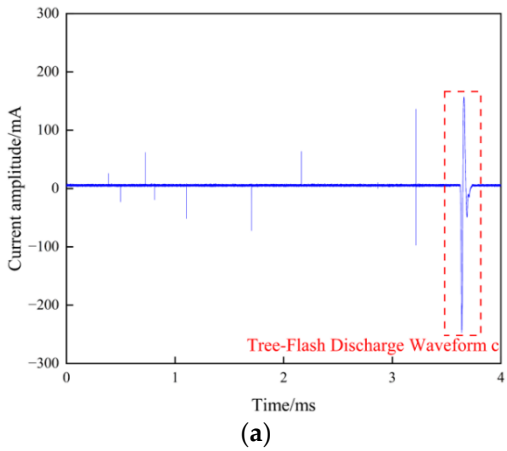

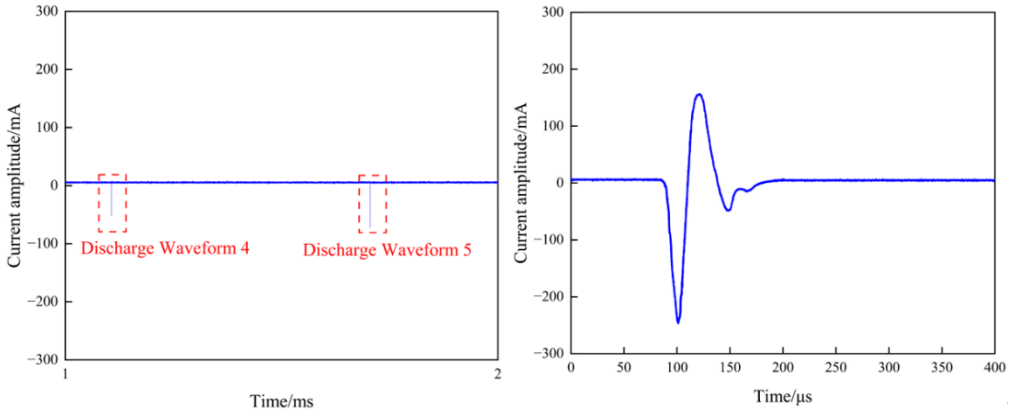

(**b**) (**c**)

Figure 6. Tree flash fault test discharge current waveform (voltage value of booster system: 110 kV). (**a**) Raw current waveform plot; (**b**) magnified view of waveform; (**c**) tree flash discharge waveform c.

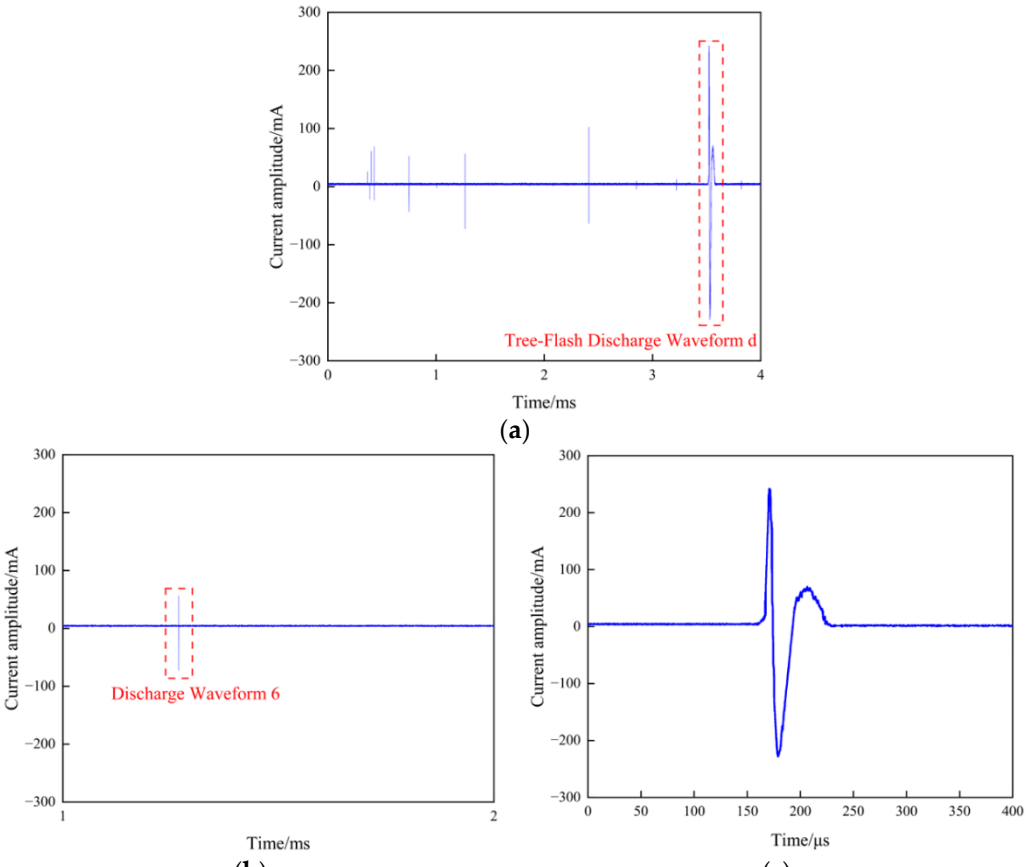

(**a**)

(**b**) (**c**)

Figure 7. Tree flash fault test discharge current waveform (voltage value of booster system: 118 kV). (**a**) Raw current waveform plot; (**b**) magnified view of waveform; (**c**) tree flash discharge waveform d.

Table 1. Peak-to-peak values and main pulse widths of tree flash discharge waveforms.

Discharge Waveform	a	b	c	d	1	2	3	4	5	6
Peak-to-peak value/mA	404.06	380.7	403.57	469.6	137.71	110.1	151.665	59.81341	80.46	128.69
main pulse width/μs	30.55	36.4	46.9	53.35	0.3	0.15	0.15	0.1	0.15	0.2

From Figures 4–7 and Table 1, it can be observed that the peak value of the transient current traveling wave signal of the tree flash fault is between −300 mA and +300 mA, with the main wave width ranging from 30 μs to 55 μs. Among them, Figure 7b has the largest

peak-to-peak value and main wave width. At t = 160.40 μs, the transient current of the tree flash fault undergoes a sudden change with an increase in amplitude. This waveform is selected to establish the model of the tree flash fault traveling wave.

Through the use of the fast Fourier transform (FFT) technique, a spectral analysis of the waveform in Figure 7b was conducted. The results, depicted in Figure 8, reveal that the tree flash fault discharge current waveform predominantly occupies the frequency range of 0 to 0.4 MHz, with a central frequency of approximately 0.025 MHz. It is observed that amplitudes are more pronounced for frequencies below 0.025 MHz, whereas between 0.025 and 0.4 MHz, the amplitudes noticeably diminish, albeit some waveforms persist.

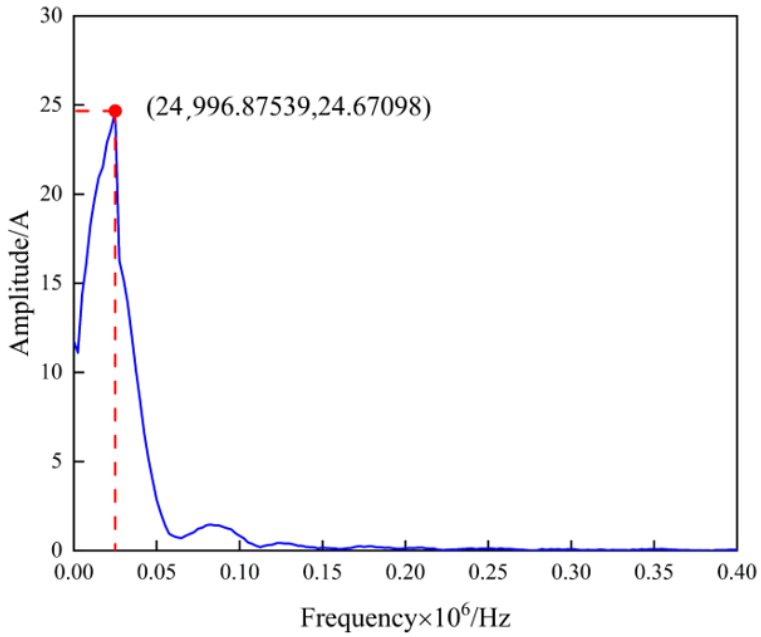

Figure 8. Tree flash fault discharge waveform spectrum.

4. Tree Flash Fault Traveling Wave Model and Attenuation Analysis

Using PSCAD/EMTDC, a three-section hybrid overhead–underground line model with a voltage level of 220 kV was constructed to investigate the frequency characteristics of tree flash fault current traveling wave attenuation. The topology of this hybrid overhead–underground line model is illustrated in Figure 9, and the specific parameters of the overhead lines and cables are listed in Table 2. The diagram of geometric parameters for the cable route is depicted in Figure 10. The cable type is "XLPE YJLV$_{22}$ 220 kV 3 × 250 mm^2". Insulator 1, Insulator 2, and Insulator 3 are, respectively, XLPE insulation, non-woven tape, and flame-retardant PVC outer sheath.

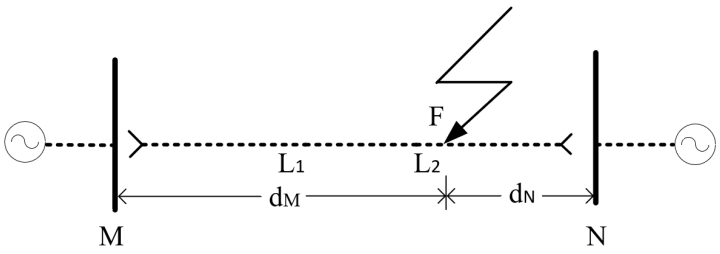

Figure 9. Topological structure of hybrid overhead–underground line model.

Table 2. Parameters of the hybrid transmission line.

Line Type	R_0/(Ω/km)	R_1/(Ω/km)	L_1/(mH/km)	L_0/(mH/km)	C_1/(μF/km)	C_0/(μF/km)
Overhead line	0.009	0.149	0.837	3.438	0.014	0.008
Power cable	0.162	0.162	0.141	0.141	0.328	0.328

R_0, R_1, L_1, L_0, C_1, and C_0 represent the zero-sequence resistance, positive-sequence resistance, positive-sequence inductance, zero-sequence inductance, positive-sequence capacitance, and zero-sequence capacitance of the line, respectively.

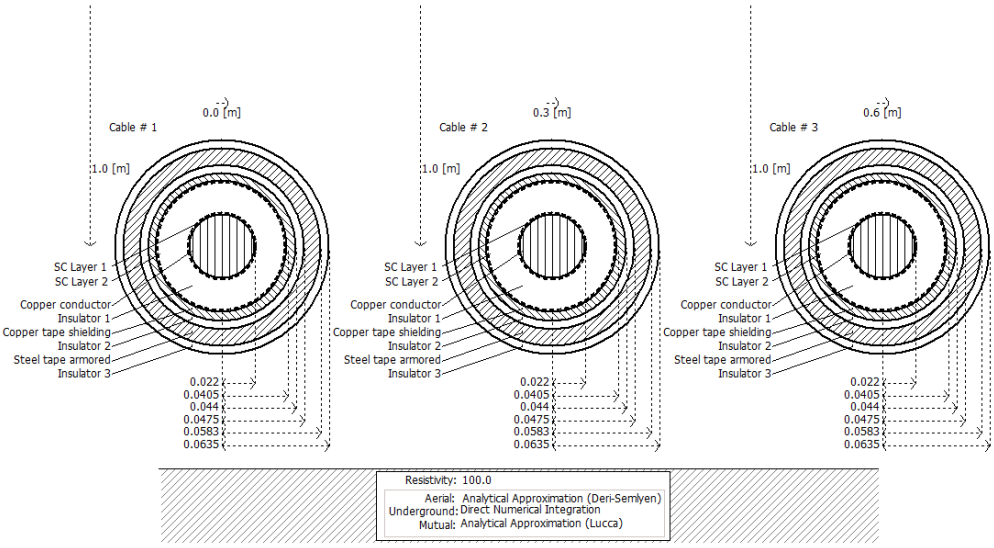

Figure 10. Presentation of the 220 kV underground cable line.

The "220 kV hybrid line" refers to a type of power transmission line with a voltage level of 220 kV. It includes both overhead sections and underground or buried cable sections. This hybrid configuration combines the characteristics of overhead lines and underground cables. It is typically used in situations where the line needs to traverse certain areas and cables need to be buried underground in specific regions. The cross-section areas of the conductors for the overhead and underground sections are 500 mm^2 and 250 mm^2, respectively. The hybrid line MN, with a length of 50 km, consists of a 20 km long overhead line ML_1, a 10 km long cable line L_1L_2, and a 20 km long overhead line L_2N.

The actual magnitude of tree flash fault currents depends on various factors, including the operating voltage of the power system, line design parameters, type and height of trees, and environmental humidity. Moreover, tree flash faults are complex phenomena, and different circumstances may result in different fault currents. For the tree itself, when a tree flash fault occurs, an arc forms on the branches, leading to the gradual carbonization of the tree. As the degree of carbonization deepens, the electrical resistance of the tree body decreases accordingly, and the transition resistance reduces, eventually falling below 1 kΩ. For a 220 kV overhead–underground hybrid line, the tree flash fault discharge current typically exceeds 220 A. This is because the arc discharge phenomenon caused by the tree flash fault increases the current to a much higher level, far exceeding the rated current of the line. As the measured current waveforms of tree flash faults have relatively low amplitudes and milliampere-level fault currents cannot significantly affect the line, the amplitude of the tree flash fault current wave is amplified to simulate the actual current magnitude when a tree flash fault occurs in the line. In PSCAD, a tree flash fault current source module is established, as shown in Figure 11, with the waveform data using the tree flash discharge waveform collected in the above experiments (Figure 7b), with an amplitude of 242.64 A.

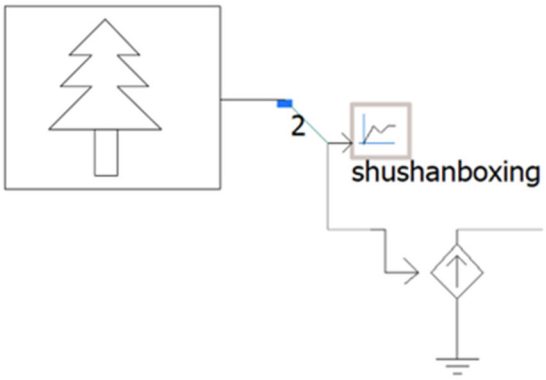

Figure 11. The tree flash fault current simulation component in PSCAD.

The tree flash fault is set at point F, located 1 km away from the L_2 end. Monitoring points are placed every 1 km towards the left from point F to record the attenuation of the tree flash fault traveling wave. The waveform characteristics at different distances are shown in Figure 12, with local magnifications depicted in Figure 13. The variation in wave amplitude attenuation is presented in Table 3.

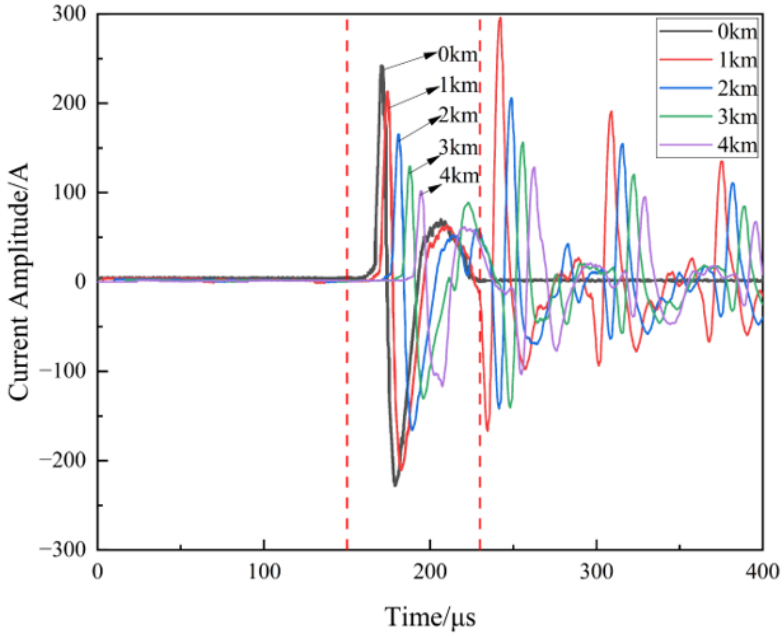

Figure 12. Characteristics of tree flash fault current waveform attenuation.

Table 3. Attenuation of tree flash fault waveform amplitude.

Distance from F Point/km	0	1	2	3	4
Current Amplitude/A	242.64	213.48	165.38	129.32	101.69
Attenuation ratio/%	-	12.02	31.84	46.70	58.09

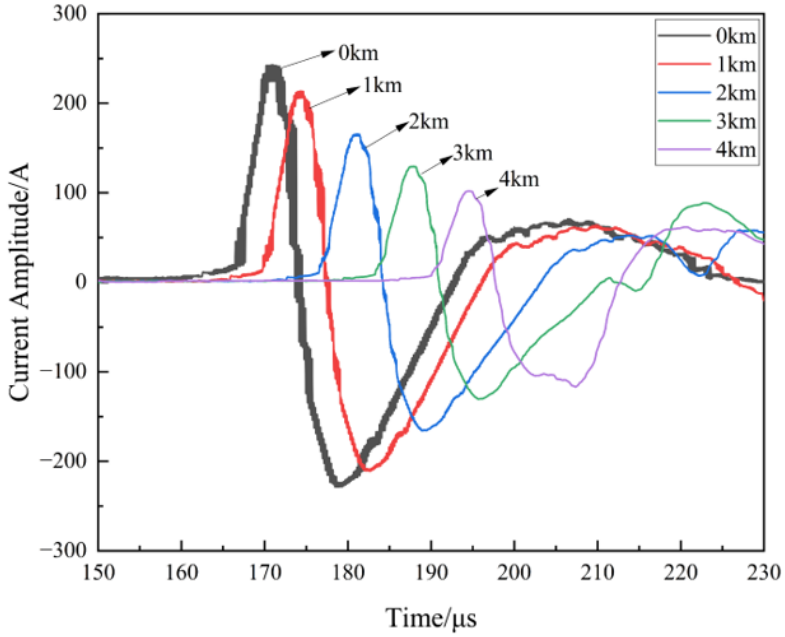

Figure 13. Localized characteristics of tree flash fault current waveform attenuation.

The attenuation of tree flash fault current waves propagating along the hybrid line is the result of various interacting factors, including electromagnetic interactions between the line and trees, frequency-dependent characteristics, electromagnetic wave loss through trees, and environmental conditions. Combining Table 3 and Figures 12 and 13, it can be observed that the attenuation of the fault current wave increases with the transmission distance. Consequently, the transition of the fault waveforms becomes smoother, and their amplitudes monotonically decrease with the transmission distance. For instance, at a distance of 1 km from the fault point F, the amplitude is 213.48 A, while at 4 km, it reduces to 101.69 A. Considering the significant attenuation of the tree flash fault current waves, this attenuation may decrease the signal strength, complicating localization. However, the traveling wave method exhibits adaptability to different attenuation environments, relying primarily on time differences in propagation rather than absolute signal strength.

5. Principles Related to Traveling Wave Detection Methods

5.1. Principles and Algorithms of Variational Modal Decomposition

VMD is a signal decomposition technique aimed at decomposing a signal into multiple intrinsic mode functions so that a local frequency component of the original signal can be represented by these intrinsic mode functions. Based on the variational principle, VMD obtains intrinsic mode functions by minimizing the total variation energy of the signal [32–34]. The variational calculation model of VMD is shown in Equation (1).

$$\begin{cases} \min\limits_{\{u_k\},\{\omega_k\}} \left\{ \sum_k \left\| \partial_t \left[\left(\delta(t) + \frac{j}{\pi t} \right) u_k(t) \right] e^{-j\omega_k t} \right\|_2^2 \right\} \\ s.t. \sum_k u_k = f \end{cases} \tag{1}$$

In the equation, $\{u_k\}$ represents the collection of various IMF components decomposed from the original signal, $\{\omega_k\}$ represents the collection of center frequencies of each IMF component, $\delta(t)$ represents the unit impulse function, and ∂_t represents the partial derivative operator.

The expanded Lagrangian expression is shown in Equation (2):

$$L\left(\{u_k\},\{\omega_k\},\lambda\right):=$$
$$\alpha\sum_k\left\|\partial_t\left[\left(\delta(t)+\frac{\mathrm{j}}{\pi t}\right)u_k(t)\right]\mathrm{e}^{-\mathrm{j}\omega_k t}\right\|_2^2 \tag{2}$$
$$+\left\|f(t)-\sum_k u_k(t)\right\|_2^2+\left\langle\lambda(t),f(t)-\sum_k u_k(t)\right\rangle$$

By introducing the Lagrange multiplier $\lambda(t)$ and the quadratic penalty term α, the problem is transformed from a constrained form into an unconstrained variational model. This extended Lagrangian expression not only simplifies the computation but also addresses the issue of estimating the fundamental frequency bandwidth.

For the "saddle point" of the extended Lagrangian expression, the alternating direction method of multipliers (ADMM) is used for computation. It iteratively optimizes the variational model by updating $\hat{u}_k^{n+1}$ and ω_k^{n+1} until the optimal solution is obtained. The expressions for the updated mode components and central frequencies are given by Equations (3) and (4):

$$\hat{u}_k^{n+1}(\omega)=\frac{\hat{f}(\omega)-\sum_{i\neq k}\hat{u}_i(\omega)+\frac{\hat{\lambda}(\omega)}{2}}{1+2\alpha(\omega-\omega_k)^2} \tag{3}$$

$$\omega_k^{n+1}(\omega)=\frac{\int_0^\infty\omega\left|\hat{u}_k(\omega)\right|^2\mathrm{d}\omega}{\int_0^\infty\left|\hat{u}_k(\omega)\right|^2\mathrm{d}\omega} \tag{4}$$

In the equations, $\hat{f}(\omega)-\sum_{i\neq k}\hat{u}_i(\omega)$ represents the current residual, $\hat{u}_k^{n+1}(\omega)$ denotes the Wiener filter of the current residual, $\omega_k^{n+1}(\omega)$ stands for the central frequency of the current mode function, and the Fourier transforms of $f(t)$, $u(t)$, $\lambda(t)$, and $\hat{u}_k^{n+1}(t)$ are, respectively, denoted by $\hat{f}(\omega)$, $\hat{u}_i(\omega)$, $\hat{\lambda}(\omega)$, and $\hat{u}_k^{n+1}(\omega)$.

5.2. Hilbert Transform

The Hilbert transform is a signal processing method that reflects the local variation characteristics of a signal. It is based on the theory of Hilbert spaces and associates the signal with an analytical function on the imaginary axis [35–37]. For a given real signal $X(t)$, its Hilbert transform $Y(t)$ can be represented as follows:

$$Y(t)=\frac{1}{\pi}P\int\frac{X(\tau)}{t-\tau}\mathrm{d}\tau \tag{5}$$

In the equation, the Cauchy principal value of the real signal $X(t)$ is denoted by P; τ and t are time variables. The essence of the Hilbert transform is to create an analytic signal by convolving with an analytical function. The real part of this analytical function is the Cauchy principal value, typically used for extracting the phase information of the signal. Convolution of the original signal with this analytical function yields the analytic signal $Z(t)$, which contains both the magnitude and phase information of the original signal. This process is akin to introducing a filter in the frequency domain, aiding in a more comprehensive understanding of the signal's characteristics. The constructed analytic signal $Z(t)$ is given by

$$Z(t)=X(t)+\mathrm{j}Y(t)=a(t)\mathrm{e}^{\mathrm{j}\varphi(t)} \tag{6}$$

In the equation, $a(t)$ represents the instantaneous amplitude of the given real signal $X(t)$, $\varphi(t)$ represents the instantaneous phase of the given real signal $X(t)$, and $\omega(t)$ represents the instantaneous frequency of the given real signal $X(t)$. The expressions for $a(t)$, $\varphi(t)$, and $\omega(t)$ are calculated accordingly:

$$a(t) = \sqrt{X^2(t) + Y^2(t)} \tag{7}$$

$$\varphi(t) = \arctan\frac{Y(t)}{X(t)} \tag{8}$$

$$\omega(t) = \frac{\mathrm{d}\varphi(t)}{\mathrm{d}t} \tag{9}$$

5.3. A Dual-End Positioning Algorithm Independent of Wave Velocity

The basic principle of the dual-end traveling wave fault location method is to utilize the propagation characteristics of the fault-generated traveling wave signal on the line and to locate the fault with the help of measurement information from both ends. The formula for calculating the fault wave velocity is given by $V = 1/\sqrt{LC}$, where C and L represent the capacitance and inductance per unit length of the line, respectively. Due to variations in wave velocity among different lines and differences caused by changes in environmental and line parameters, the numerical values of wave velocities at different times and positions on the same line will also differ.

By employing the Karhunen–Loève transform, when a fault occurs in a mixed-line power system, the fault traveling wave signal can be decoupled into line-mode and zero-mode components, with the wave velocity values of the zero-mode component set to v_0 and the line-mode component set to v_1. Through the propagation process of the fault traveling wave's zero mode and line-mode components on the mixed line, the following formula for calculating the positioning distance can be obtained:

$$\begin{cases} l_{\mathbf{MN}} = v_1(t_{\mathbf{M1}} - t_0 + t_{\mathbf{N1}} - t_0) \\ l_{\mathbf{MN}} = v_0(t_{\mathbf{M0}} - t_0 + t_{\mathbf{N0}} - t_0) \\ v_0(t_{\mathbf{M0}} - t_0) = v_1(t_{\mathbf{M1}} - t_0) \end{cases} \tag{10}$$

The calculation formula obtained after eliminating equations v_1, t_0, and v_0 is (11):

$$d_{\mathrm{M}} = \frac{t_{\mathrm{Mo}} - t_{\mathrm{M1}}}{t_{\mathrm{Mo}} - t_{\mathrm{M1}} + t_{\mathrm{N0}} - t_{\mathrm{N1}}} l_{\mathrm{MN}} \tag{11}$$

In the equation, t_{Mo} and t_{N0} represent the time for zero-mode traveling waves to reach the ends M and N, respectively; t_{M1} and t_{N1} represent the time for line-mode traveling waves to reach the ends M and N, respectively; v_1 and v_0 represent the velocity values of the line-mode and zero-mode traveling waves, respectively; l_{MN} represents the length of line MN; and t_0 represents intermediate parameters.

The model defined by Equations (10)–(12) is newly introduced in this work. The positioning results of this algorithm are independent of the wave velocity and changes in line parameters. Moreover, it does not require measuring and recording the occurrence time of fault reflection waves, thereby reducing the difficulty of wavefront exploration and enhancing the accuracy of fault positioning.

6. Tree Flash Fault Location Simulation Analysis

In the experimental setup, we initially acquired the signal data of tree flash faults. These signal data may contain rich frequency components and temporal characteristics,

requiring further analysis and processing. Through HHT, we can decompose the signal into Intrinsic Mode Functions (IMFs) and obtain the instantaneous frequency information of each IMF. The key to associating HHT with the experimental setup is to ensure that the HHT transformation accurately reflects the characteristics and variations of the tree flash fault signals. Therefore, selecting the Butterworth filter as the implementation algorithm for the HHT filter is crucial. The Butterworth filter is a common digital filter with smooth frequency response characteristics, suitable for smoothing signal processing to reduce interference and highlight the main frequency components. The filtered signal retains important frequency components of the tree flash fault signal while filtering out unwanted frequency components and noise. The implementation of HHT mainly involves IMF decomposition and instantaneous frequency extraction. The decomposition of IMFs uses the Empirical Mode Decomposition (EMD) method, which decomposes the signal into a series of Intrinsic Mode Functions. Each IMF represents an inherent vibration mode of the signal. The extraction of instantaneous frequency can be achieved through the Hilbert transform. HT is a mathematical tool used to calculate the instantaneous frequency of a signal, which can extract the instantaneous frequency from the analytic signal of the original signal. Finally, combining EMD and HT forms the Hilbert–Huang transform. This transformation can extract instantaneous frequency from the original signal to better understand the signal's time-frequency characteristics.

The simulation model adopts the hybrid line model shown in Figure 9. The tree flash fault is set on the overhead line of the hybrid line M-end, 38 km away. The occurrence time of the tree flash fault is set to 2 μs, and the tree flash fault wave signal is decoupled. When selecting the VMD decomposition parameter K value, refer to the Optimal Variational Mode Decomposition (OVMD) algorithm and set the K value to 4. The settings for other VMD parameters are as follows: penalty factor alpha = 8000; convergence tolerance tol = 0.000001. The zero-mode component after decoupling is subjected to VMD decomposition, and the decomposition result is shown in Figure 14.

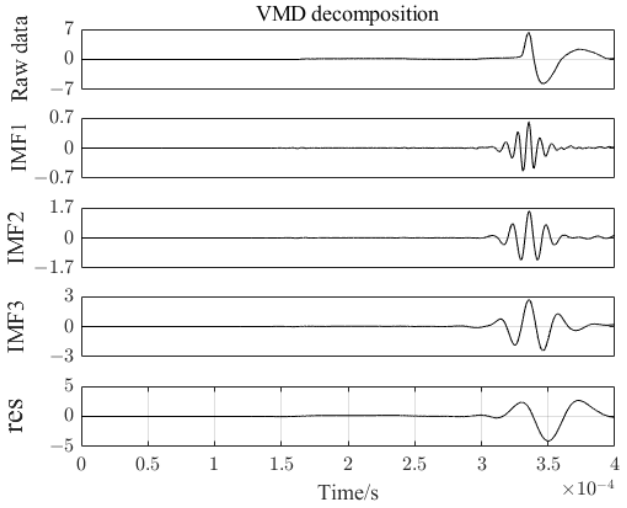

Figure 14. The measured zero-mode component at terminal M and its VMD decomposition results.

From Figure 14, it can be observed that the first sequence represents the amplitude of the decoupled zero-mode component of the original signal, while the last sequence represents the residual component trend term. The three intermediate sequences represent the intrinsic mode functions obtained after VMD decomposition, namely IMF1 to IMF3, arranged in descending order of frequency from high to low. The variation trend of the IMF3 component exhibits the closest resemblance to the original zero-mode component.

Figure 15 illustrates the variation of the instantaneous frequency of the IMF3 component signal obtained through the Hilbert transform. The time of the initial traveling wave

of the tree flash fault is determined by the abrupt point of the first instantaneous frequency.

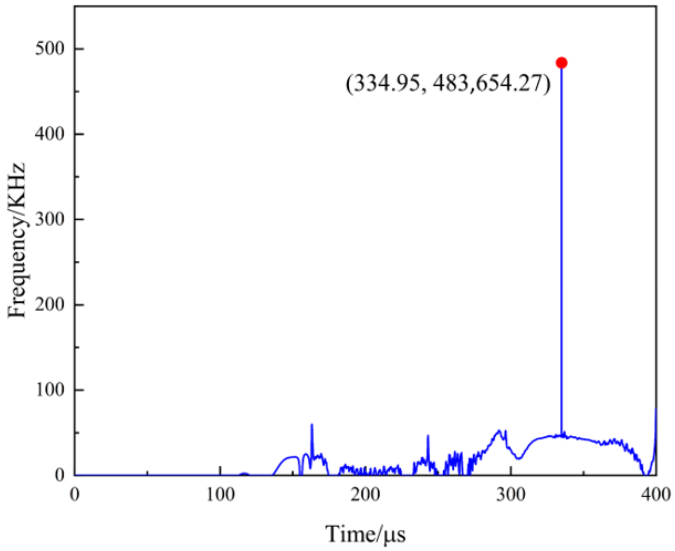

Figure 15. The VMD-Hilbert transform results of the zero-mode component at measurement terminal M.

From Figure 15, it can be observed that the frequency of the first instantaneous frequency abrupt point of the zero-mode component is 55,653.2 Hz, and the corresponding time is 334.95 μs. Therefore, the time for the zero-mode component of the tree flash fault traveling wave to reach terminal M is 334.95 μs.

Similarly, it can be inferred that the zero-mode component at measurement terminal N and its VMD decomposition results are shown in Figure 16. The VMD-Hilbert transform results are depicted in Figure 17, indicating that the time for the zero-mode component to reach terminal N is 255.9 μs.

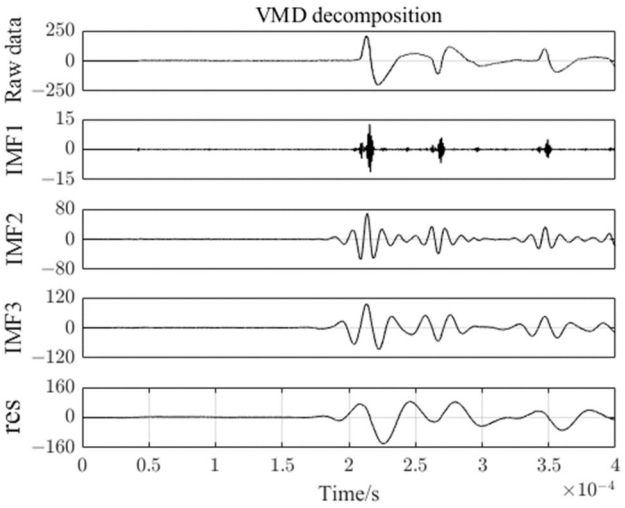

Figure 16. The zero-mode signal at measurement terminal N and its VMD decomposition results.

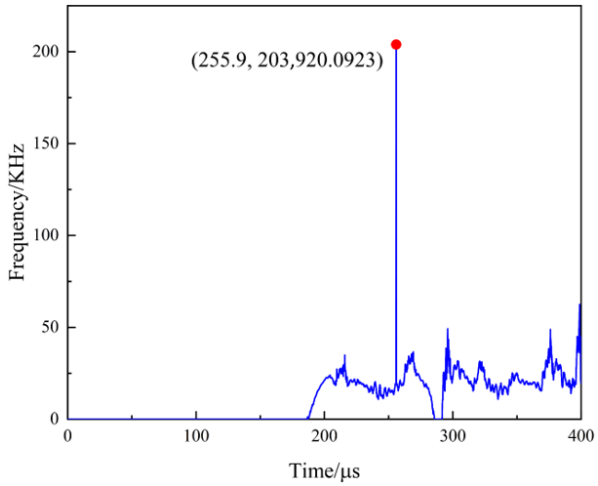

Figure 17. The VMD-Hilbert transform results of the zero-mode component at measurement terminal N.

The line-mode component at measurement terminal M and its VMD decomposition results are shown in Figure 18. The VMD-Hilbert transform results are illustrated in Figure 19, indicating that the time for the line-mode component to reach terminal M is 163.4 μs.

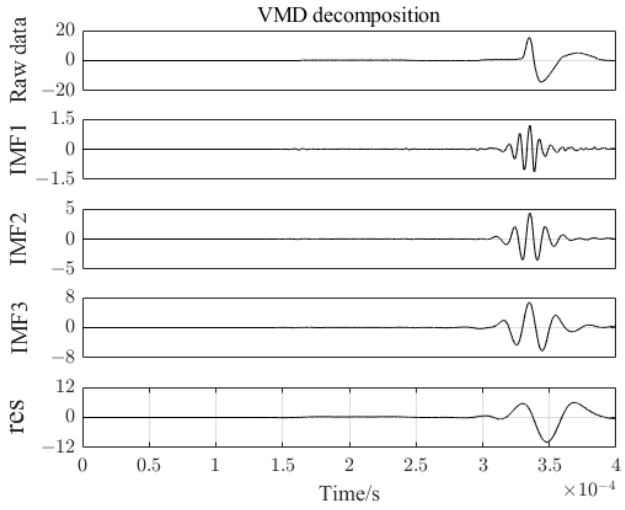

Figure 18. The line-mode component at measurement terminal M and its VMD decomposition results.

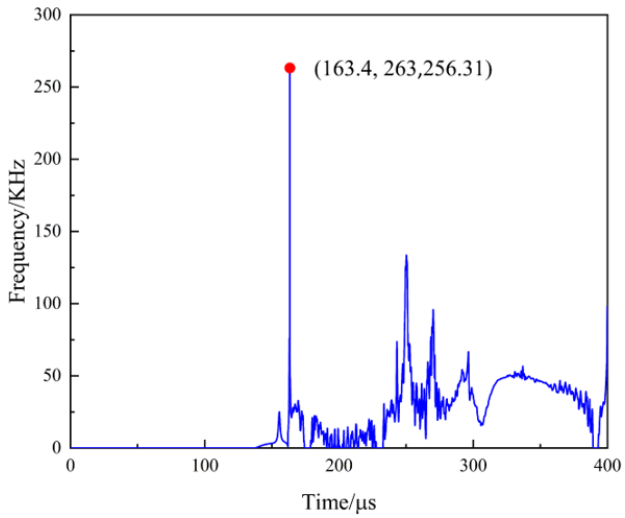

Figure 19. The VMD-Hilbert transform results of the line-mode component at measurement terminal M.

The line-mode component at measurement terminal N and its VMD decomposition results are shown in Figure 20. The VMD-Hilbert transform results are depicted in Figure 21, indicating that the time for the line-mode component to reach terminal N is 202.3 μs.

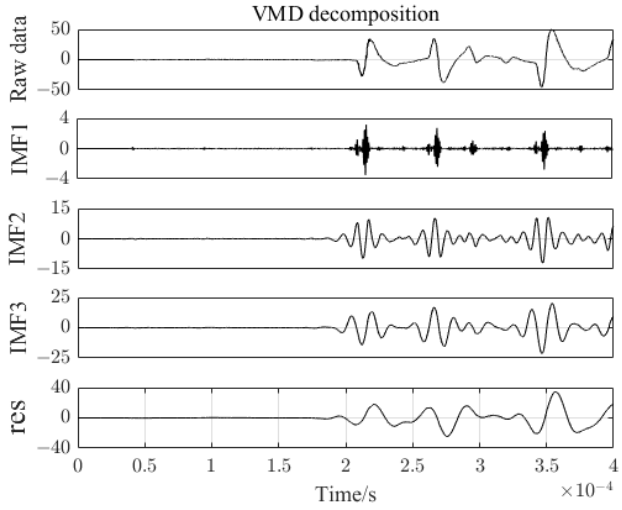

Figure 20. The line-mode component at measurement terminal N and its VMD decomposition results.

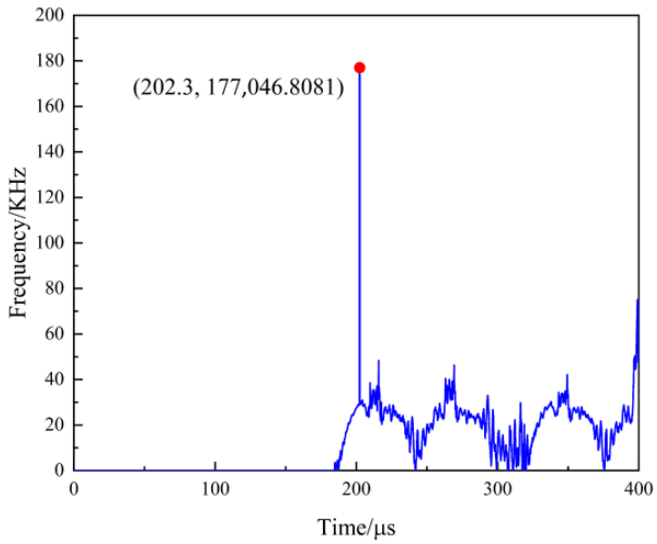

Figure 21. The VMD-Hilbert transform results of the line-mode component at measurement terminal N.

Substituting the four time data into Equation (11):

$$d_M = \frac{(334.95 - 163.4) \times 50}{334.95 - 163.4 + 255.9 - 202.3} = 38.097\,\text{km}$$

It can be observed that the deviation from the actual tree flash fault location, which is 38 km away from terminal *M*, is 97 m. This meets the requirement for precise localization of the tree flash fault point.

Based on the calculation formula of the propagation speed of tree flash fault traveling waves on overhead lines and cables derived from the hybrid line model's parameters of inductance, capacitance, and the wave velocity of transient faults, the propagation speed of the tree flash fault traveling wave on the overhead line is denoted as $V_J = 2.92128046 \times 10^8$ m/s, and on the cable as $V_D = 1.47046104 \times 10^8$ m/s. Since the lengths of the overhead line and cable of the hybrid line and the values of the wave velocity are

known, according to the formula $t = l/v$, the travel times of the tree flash fault traveling wave on the overhead line segments ML_1 and L_2N can be, respectively, calculated as $t_a = 6.846312867 \times 10^{-5}$ s, and on the cable segment L_1L_2, they can be calculated as $t_b = 6.800588202 \times 10^{-5}$ s.

Using Equation (12), the distance of the tree flash fault point from terminal *M* is calculated to be 37.867 km, with an error of 133 m. By comparing the two methods, it can be concluded that the wave-based positioning method, independent of wave speed, exhibits higher positioning accuracy and better meets the requirement for precise localization of tree flash faults.

$$d_M = d_{ML_1} + L_1L_2 + (\mathrm{t}_{M1} - t_a - t_b)V_J \tag{12}$$

At positions 20 km, 25 km, 30 km, 35 km, and 45 km from terminal M, simulation experiments were conducted to introduce tree flash faults. The localization of the tree flash fault was performed using both the method combining VMD decomposition and Hilbert transform and the formula-based wave-speed-based double-end positioning method. The calculated results of the tree flash fault point positions are presented in Tables 4 and 5.

Table 4. The localization method combines VMD decomposition and Hilbert transform.

Fault Distance/km	Calculated Distance/km	Inaccuracies/km
20	19.965	−0.039
25	25.023	0.023
30	29.963	−0.037
35	35.070	0.070
45	44.884	−0.116

Table 5. Traditional wave-speed-based double-end positioning method.

Fault Distance/km	Calculated Distance/km	Inaccuracies/km
20	19.925	−0.075
25	25.065	0.065
30	30.908	0.908
35	35.102	0.102
45	44.858	−0.142

By analyzing the data in the table, it can be concluded that the tree flash fault localization method utilizing VMD decomposition and Hilbert transform is effective in pinpointing tree flash fault points. Moreover, as the occurrence position of the tree flash fault point moves closer to terminals M and N, the localization error shows a trend of gradual increase.

Capturing phase currents may be more practically feasible in real-world applications, and it is a more common practice to collect phase currents for fault extraction, especially in the presence of loaded distributed transformers. In future practical studies, we will consider collecting phase current data and attempt to extract fault information from it to make our research more relevant to real-world scenarios and improve the applicability and reliability of our method. Although the tree flash fault localization method utilizing VMD decomposition and Hilbert transform achieves higher accuracy, it may face complex scenarios and conditions in practical applications. Further algorithm optimization is required to enhance its applicability and robustness in diverse environments. Regarding the tree flash fault discharge test platform and hybrid line simulation system, consideration should be given to introducing more advanced equipment and techniques optimizing experimental designs and simulation models to improve the accuracy and reliability of experiments, thereby further validating the effectiveness of the research outcomes.

7. Conclusions

This paper conducted experimental research on tree flash fault discharges, collecting waveform data of tree flash fault discharge currents. Subsequently, the waveforms were analyzed in both time and frequency domains, and a tree flash fault traveling wave model was established to analyze its transmission attenuation characteristics. Finally, the localization of tree flash fault positions was studied, yielding the following conclusions.

During the tree flashover fault discharge experiments, various forms of tree flashover fault discharge current waveforms were observed, and their spectral characteristics were thoroughly investigated. It was found that the initial segment amplitude of the tree flashover fault discharge current waveform before the abrupt change point was relatively low, followed by the appearance of large positive and negative alternating pulses after the change point. The peak value of the transient current traveling wave signal during the tree flashover fault ranged from −300 mA to 300 mA, with the main pulse width ranging from 30 μs to 55 μs. The frequency of the tree flashover fault current waveform was mainly concentrated between 0 and 0.4 MHz, with a center frequency of around 0.02 MHz. Through experimental research, abundant data and results were obtained, providing support for further research on tree flashover fault localization.

In terms of system modeling, models were established for overhead lines, cable systems, and tree flashover fault traveling wave characteristics. These models were integrated into an overall simulation system for hybrid overhead–underground lines. Through simulation analysis of the attenuation characteristics of tree flashover fault traveling waves, it was determined that the amplitude of the tree flashover fault current traveling wave decreases monotonically with transmission distance and at a relatively high rate. Additionally, the transition of the waveform is more gradual. This provides theoretical support and method selection for subsequent tree flashover fault localization.

Compared to the traditional wave-speed-based double-end traveling wave positioning method, the tree flash fault localization method utilizing VMD decomposition and Hilbert transform demonstrates higher positioning accuracy. This indicates the accuracy and effectiveness of this method in tree flash fault localization, providing theoretical and practical support for the detection and localization of tree flash faults in the future.

Author Contributions: Z.H., C.F., Q.J., T.H., and J.L. conceived the idea and designed the experiments. Z.H., C.F., and Q.J. led the experiments. T.H. and J.L. contributed to the data analysis. Z.H. and C.F. wrote the paper. All authors have read and agreed to the published version of the manuscript.

Funding: This research is funded by the National Natural Science Foundation (project name: Study on the Impact Mechanism and Regulation of Large Suspended Potential Conductors on Air Gap Operation Impulse Discharge Characteristics; project contract number: 51807110).

Data Availability Statement: The raw data supporting the conclusions of this article will be made available by the authors on request.

Acknowledgments: We Thank Chong Cao for his contribution to the data analysis. We would like to thank the editor and the anonymous reviewers for their helpful suggestions and comments.

Conflicts of Interest: The authors declare no conflicts of interest.

References

1. Liu, H. Research on Tree Flash Failure Analysis and Tree Line Distance Prediction Method for Transmission Line. *J. Electr. Eng.* **2019**, *7*, 92–97.
2. Kakareko, G.; Jung, S.; Ozguven, E.E. Estimation of tree failure consequences due to high winds using convolutional neural networks. *Int. J. Remote Sens.* **2020**, *41*, 9039–9064. https://doi.org/10.1080/01431161.2020.1797219.
3. Wu, J.; Liu, H.; Yang, J.; Chen, Y. Tree barrier prediction of power lines based on tree height growth model. *IOP Conf. Ser. Earth Environ. Sci.* **2021**, *645*, 012008.

4. Jamborsalamati, P.; Moghimi, M.; Hossain, M.J.; Taghizadeh, S.; Lu, J.; Konstantinou, G. A Framework for Evaluation of Power Grid Resilience Case Study: 2016 South Australian Blackout. In Proceedings of the 2018 IEEE International Conference on Environment and Electrical Engineering and 2018 IEEE Industrial and Commercial Power Systems Europe (EEEIC/I&CPS Europe), Palermo, Italy, 12–15 June 2018; pp. 1–6.
5. Abu-Rub, O.H.; Fard, A.Y.; Umar, M.F.; Hosseinzadehtaher, M.; Shadmands, M.B. Towards Intelligent Power Electronics-Dominated Grid via Machine Learning Techniques. *IEEE Power Electron. Mag.* **2021**, *8*, 28–38. https://doi.org/10.1109/MPEL.2020.3047506.
6. Goodfellow, J. *Investigating Tree-Caused Faults*; Transmission & Distribution World: New York, NY, USA, 2005.
7. Yi, C.W.; Yu-Hsing, W.; Wai, C.S.; Siang, T.P.; Ling, L.M.; Lun, L.H.; Jimmy, W.; Man, L.Y. AI-IoT integrated framework for tree tilt monitoring: A case study on tree failure in Hong Kong. *Agric. For. Meteorol.* **2023**, *341*, 109678.
8. Zhang, L.Y.; Xian, X.Y. Research on Prevention of Cascading Failures Based on Time of Vegetation-Related Failure. *Appl. Mech. Mater.* **2013**, *2388*, 1392–1395. https://doi.org/10.4028/www.scientific.net/AMM.321-324.1392.
9. Jahani, A.; Saffariha, M. Tree failure prediction model (TFPM): Machine learning techniques comparison in failure hazard assessment of Platanus orientalis in urban forestry. *Nat. Hazards* **2021**, *110*, 881–898. https://doi.org/10.1007/S11069-021-04972-7.
10. Liu, Z.; Gao, S.; Jiang, H.; Guo, R.; Kang, Y.; Chen, X. *Mechanism Analysis and Experimental Study on Tree Faults in Transmission Lines*; IOP Publishing: Chongqing, China, 2019; pp. 9–14.
11. Sadegh, B.; Ashkan, S.; Mohammad, R. Outage Cause Detection in Power Distribution Systems based on Data Mining. *IEEE Trans. Ind. Inform.* **2020**, *17*, 640–649. https://doi.org/10.1109/tii.2020.2966505.
12. Melagoda, A.U.; Karunarathna, T.D.L.P.; Nisaharan, G.; Amarasinghe, P.A.G.M.; Abeygunawardane, S.K. Application of Machine Learning Algorithms for Predicting Vegetation Related Outages in Power Distribution Systems. In Proceedings of the 2021 3rd International Conference on Electrical Engineering (EECon), Colombo, Sri Lanka, 24 September 2021; pp. 25–30.
13. Bahador, N.; Namdari, F.; Matinfar, H.R. Modelling and detection of live tree-related high impedance fault in distribution systems. *IET Gener. Transm. Distrib.* **2018**, *12*, 756–766. https://doi.org/10.1049/iet-gtd.2017.0211.
14. Bahador, N.; Namdari, F.; Matinfar, H.R. Tree-related high impedance fault location using phase shift measurement of high frequency magnetic field. *Int. J. Electr. Power Energy Syst.* **2018**, *100*, 531–539. https://doi.org/10.1016/j.ijepes.2018.03.008.
15. Ashok, V.; Yadav, A. Fault Diagnosis Scheme for Cross-Country Faults in Dual-Circuit Line with Emphasis on High-Impedance Fault Syndrome. *IEEE Syst. J.* **2020**, *15*, 2087–2097. https://doi.org/10.1109/jsyst.2020.2991770.
16. Hassan, O.E.; Amer, M.; Abdelsalam, A.K.; Williams, B.W. Induction motor broken rotor bar fault detection techniques based on fault signature analysis—A review. *IET Electr. Power Appl.* **2018**, *12*, 895–907. https://doi.org/10.1049/iet-epa.2018.0054.
17. Cui, H.; Guan, Y.; Chen, H.; Deng, W. A Novel Advancing Signal Processing Method Based on Coupled Multi-Stable Stochastic Resonance for Fault Detection. *Appl. Sci.* **2021**, *11*, 5385. https://doi.org/10.3390/APP11125385.
18. Patel, B. A new FDOST entropy based intelligent digital relaying for detection, classification and localization of faults on the hybrid transmission line. *Electr. Power Syst. Res.* **2018**, *157*, 39–47. https://doi.org/10.1016/j.epsr.2017.12.002.
19. Li, W.; Deka, D.; Chertkov, M.; Wang, M. Real-Time Faulted Line Localization and PMU Placement in Power Systems Through Convolutional Neural Networks. *IEEE Trans. Power Syst.* **2019**, *34*, 4640–4651. https://doi.org/10.1109/tpwrs.2019.2917794.
20. Fahim, S.R.; Sarker, Y.; Islam, O.K.; Sarker, S.K.; Ishraque, M.F.; Das, S.K. An Intelligent Approach of Fault Classification and Localization of a Power Transmission Line. In Proceedings of the 2019 IEEE International Conference on Power, Electrical, and Electronics and Industrial Applications (PEEIACON), Dhaka, Bangladesh, 29 November–1 December 2019; pp. 53–56.
21. Zakaria, E.M.; Niroop, S.; Prakash, R.; Shrirang, A. Random Forest Regressor-Based Approach for Detecting Fault Location and Duration in Power Systems. *Sensors* **2022**, *22*, 458. https://doi.org/10.3390/S22020458.
22. Shu, H.; Liu, X.; Tian, X. Single-Ended Fault Location for Hybrid Feeders Based on Characteristic Distribution of Traveling Wave Along a Line. *IEEE Trans. Power Deliv.* **2020**, *36*, 339–350. https://doi.org/10.1109/tpwrd.2020.2976691.
23. Tashakkori, A.; Wolfs, P.J.; Islam, S.; Abu-Siada, A. Fault Location on Radial Distribution Networks via Distributed Synchronized Traveling Wave Detectors. *IEEE Trans. Power Deliv.* **2019**, *35*, 1553–1562. https://doi.org/10.1109/tpwrd.2019.2948174.
24. Wang, J.; Zhang, Y. Traveling Wave Propagation Characteristic-Based LCC-MMC Hybrid HVDC Transmission Line Fault Location Method. *IEEE Trans. Power Deliv.* **2022**, *37*, 208–218. https://doi.org/10.1109/TPWRD.2021.3055840.
25. Ding, J.; Wang, X.; Zheng, Y.; Li, L. Distributed Traveling-Wave-Based Fault-Location Algorithm Embedded in Multiterminal Transmission Lines. *IEEE Trans. Power Deliv.* **2018**, *33*, 3045–3054. https://doi.org/10.1109/tpwrd.2018.2866634.
26. Wang, L.; Liu, H.; Dai, L.; Liu, Y. Novel Method for Identifying Fault Location of Mixed Lines. *Energies* **2018**, *11*, 1529. https://doi.org/10.3390/en11061529.
27. Naidu, O.; Pradhan, A.K. A Traveling Wave-Based Fault Location Method Using Unsynchronized Current Measurements. *IEEE Trans. Power Deliv.* **2019**, *34*, 505–513. https://doi.org/10.1109/TPWRD.2018.2875598.
28. Lopes, F.V.; Leite, E.J. Traveling Wave-Based Solutions for Transmission Line Two-Terminal Data Time Synchronization. *IEEE Trans. Power Deliv.* **2018**, *33*, 3240–3241. https://doi.org/10.1109/tpwrd.2018.2831458.
29. Yu, K.; Zeng, J.; Zeng, X.; Liu, F.; Zu, Y.; Yu, Q.; Zhuo, C. A novel traveling wave fault location method for transmission network based on time linear dependence. *Int. J. Electr. Power Energy Syst.* **2021**, *126*, 106608. https://doi.org/10.1016/j.ijepes.2020.106608.
30. Zhang, C.; Song, G.; Wang, T.; Yang, L. Single-Ended Traveling Wave Fault Location Method in DC Transmission Line Based on Wave Front Information. *IEEE Trans. Power Deliv.* **2019**, *34*, 2028–2038. https://doi.org/10.1109/TPWRD.2019.2922654.

31. Liu, Z.Y.; Tan, F.L.; Kang, Y.B.; Song, Z.Q.; Guo, R.; Hu, F. Mechanism Analysis and Experimental study of Transmission Line Tree-related Failures. *Electr. Power Eng. Technol.* **2017**, *36*, 122–126. https://doi.org/10.19464/j.cnki.cn32-1541/tm.2017.06.022.
32. Zhang, Y.; Chen, B.; Pan, G.; Zhao, Y. A novel hybrid model based on VMD-WT and PCA-BP-RBF neural network for short-term wind speed forecasting. *Energy Convers. Manag.* **2019**, *195*, 180–197. https://doi.org/10.1016/j.enconman.2019.05.005.
33. Ding, J.; Xiao, D.; Li, X. Gear Fault Diagnosis Based on Genetic Mutation Particle Swarm Optimization VMD and Probabilistic Neural Network Algorithm. *IEEE Access* **2020**, *8*, 18456–18474. https://doi.org/10.1109/access.2020.2968382.
34. Sun, Z.; Zhao, S.; Zhang, J. Short-Term Wind Power Forecasting on Multiple Scales Using VMD Decomposition, K-Means Clustering and LSTM Principal Computing. *IEEE Access* **2019**, *7*, 166917–166929. https://doi.org/10.1109/ACCESS.2019.2942040.
35. de Souza, U.B.; Escola, J.P.; da Cunha Brito, L. A survey on Hilbert-Huang transform: Evolution, challenges and solutions. *Digit. Signal Process.* **2022**, *120*, 103292. https://doi.org/10.1016/J.DSP.2021.103292.
36. Wang, Y.; Li, Q.; Zhou, F.; Zhou, Y.; Mu, X. A New Method With Hilbert Transform and Slip-SVD-Based Noise-Suppression Algorithm for Noisy Power Quality Monitoring. *IEEE Trans. Instrum. Meas.* **2019**, *68*, 987–1001.
37. Guo, M.-F.; Yang, N.-C.; Chen, W.-F. Deep-Learning-Based Fault Classification Using Hilbert–Huang Transform and Convolutional Neural Network in Power Distribution Systems. *IEEE Sens. J.* **2019**, *19*, 6905–6913. https://doi.org/10.1109/jsen.2019.2913006.